〔農工研技報　216
9 ～ 19，2014〕

Numerical Estimation of the Vertical Fecal Coliforms Distribution in Reservoirs

HAMADA Koji*, SHIRATANI Eisaku**,
KUBOTA Tomijiro* and HITOMI Tadayoshi*

*Hydraulic Engineering Research Division, Water Environment
**Department of Planning and General Administration, Senior Research Coordinator

Keywords: vertical one-dimensional layer model, fecal coliforms, vertical profile

Ⅰ Introduction

Fecal contamination of irrigation water is responsible for the spread of many contagious diseases (WHO, 2006), and agricultural activity can increase infection risks for farmers and consumers of crops. Fecal bacteria in human and animal waste may contain some pathogenic organisms on rare occasions. Some agricultural reservoirs in Japan (particularly those in the middle reaches of river basins) receive runoff from residential areas and stock farms, and such runoff is at a risk to contaminating of fecal bacteria in irrigation water. Accordingly, understanding the dynamics of fecal bacteria in such reservoirs is critical for the prevention and management of fecal contamination of irrigation water.

Fecal coliforms (FC), which have been utilized as indicators of fecal contamination, have been shown to exhibit vertical fluctuations within an agricultural reservoir (Hamada *et al*., 2010). Vertical profiles describing FC concentration are used in the management of reservoir intake, and it is possible that differences in intake depth may result in differences in risk for farmers and consumers of crops, yet the mechanisms underlying the vertical distribution of FC remain unknown. Therefore, further studies are required to improve understanding of the distribution of fecal bacteria.

Ecological modeling is one of the most effective means of investigating the ecological mechanisms at work in the water environment. Previously, ecological models incorporating the behavior of fecal bacteria have been adapted for investigation of wastewater treatment plants (e.g., Suh *et al*., 2009), coastal lagoons (e.g., Steets and Holden, 2003), and lakes (e.g., Canale *et al*., 1993). However, previous studies have targeted primarily the horizontal and temporal distributions of fecal bacteria in water bodies and have neglected to consider the vertical distributions of fecal bacteria in water bodies in any great detail.

Many numerical models have been developed for the investigation of reservoirs and lakes, including one-dimensional, vertical/horizontal two-dimensional, and three-dimensional models. All models developed previously are associated with some advantages and disadvantages, although an appropriate model can usually be selected according to the specific aims of a given study. Fecal bacteria such as coliforms move through water bodies in two ways: they can be considered to be free-floating or particle-attached types (Chapra, 1997). In this context, it is important to consider the movements of such particles within reservoirs when constructing vertical profiles of fecal bacteria. Aki *et al*. (1981) used a vertical one-dimensional model to simulate a vertical turbidity profile in a reservoir, and vertical one-dimensional models have been used widely for the simulation of vertical water quality profiles in reservoirs and lakes. For example, Momii and Ito (2008) used such a model for the simulation of water temperature in a reservoir in Japan. In general, vertical one-dimensional models have achieved positive results in reservoir settings, demonstrating their applicability for investigation of the mechanisms controlling the vertical distribution of FC in reservoirs.

In the present study, the vertical distribution of FC is simulated using a vertical one-dimensional layer model. In particular, FC are separated into free-floating and particle-attached fractions to simulate the effects of differences on density of free-FC or flocks, particle size and sensitivity for solar radiation.

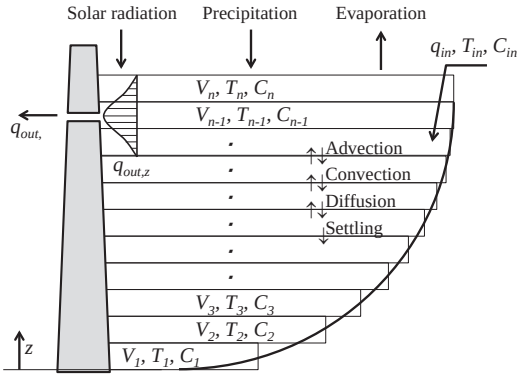

Fig.1 Vertical one-dimensional layer model of reservoir

Ⅱ Model Structure

2.1 Vertical one-dimensional layer model

The present study adopts a vertical one-dimensional layer model that was designed to calculate temperature and can simulate the distribution of indicators of fecal bacteria. **Figure 1** illustrates the framework of the model. The reservoir in the model is constructed from horizontally partitioned layers and the model calculates flow, heat, and mass balances in each layer. Surface areas and storage volumes are calculated as functions of water depth based on rating curves. Although the number of layers is fixed and all layers exhibit equal thickness, this thickness is not fixed, and it is determined by each calculation step according to the water level the reservoir.

The basic equations adopted to describe flow, heat, and mass conservation in the model at height z are as follows.

$$\frac{\partial Av}{\partial t} = q_{in} - q_{out}\ , \tag{1}$$

$$\frac{\partial T}{\partial t} = \frac{1}{A}\left(q_{in}T_{in} - q_{out}T\right) - \frac{1}{A}\frac{\partial}{\partial z}\left(vAT\right) + \frac{D_T}{A}\frac{\partial}{\partial z}\left(A\frac{\partial T}{\partial z}\right) + \frac{1}{\rho_w cA}\frac{\partial}{\partial z}\left(A\phi\right)\ , \tag{2}$$

$$\frac{\partial C}{\partial t} = \frac{1}{A}\left(q_{in}C_{in} - q_{out}C\right) - \frac{1}{A}\frac{\partial}{\partial z}\left(vAC\right) + \frac{D_C}{A}\frac{\partial}{\partial z}\left(A\frac{\partial C}{\partial z}\right) + \frac{\partial}{\partial z}\left(wC\right) + \mu C\ . \tag{3}$$

Here, v is the vertical velocity of water (m h^{-1}), A is the horizontal water area of the reservoir (m^2), and q_{in} and q_{out} are the inflow and discharge, respectively, of the reservoir (m^3 h^{-1}). T is water temperature in the reservoir (°C), T_{in} is the water temperature at the inflow (°C), D_T is a heat diffusion coefficient (m^2 h^{-1}), ρ_w is water density (g cm^{-3}), c is the specific heat of water (4.184 kJ kg^{-1} $degree^{-1}$), ϕ is radiation heat (J m^{-2} h^{-1}), C is water quality in the reservoir (mg L^{-1} or MPN (100 mL)$^{-1}$), C_{in} is water quality at the inflow (mg L^{-1} or MPN (100 mL)$^{-1}$), D_C is a water quality diffusion coefficient (m^2 h^{-1}), μ is the specific reaction rate (d^{-1}), and w is the settling velocity (m h^{-1}).

2.2 Inflow and discharge

Inflow and discharge for each layer are calculated according to a Gaussian distribution using inflow depth and discharge depth as mode depths following equations as entrainment flows. Inflow depth is determined by comparing water densities between the inflowing river and each layer, assuming that water density at the inflow corresponds to that of the inflowing river. Water intake depth is determined using the actual depth of the intake from the reservoir. Accordingly,

$$q_{i/o} = A\exp\left[-\frac{\left(z - z_{i/o}\right)^2}{2\delta_{i/o}^2}\right] \Bigg/ \int_{bottom}^{surface} A\exp\left[-\frac{\left(z - z_{i/o}\right)^2}{2\delta_{i/o}^2}\right]dz \cdot Q_{i/o}\ , \tag{4}$$

where $q_{i/o}$ is inflow/discharge (m^3 h^{-1}), $z_{i/o}$ is inflow/discharge height (m), $Q_{i/o}$ is total inflow/discharge (m^3 h^{-1}), and $\delta_{i/o}$ is the flow thickness associated with inflow/discharge (m). Equations 5 and 6 describe inflow and discharge, respectively:

$$\delta_{in} = \frac{1}{3.92}\left(\frac{q_{in}}{G\theta\sqrt{g\varepsilon}}\right)^{1/2}, \tag{5}$$

$$\delta_{out} = \frac{1}{3.92}\left(\frac{q_{out}}{G\theta\sqrt{g\varepsilon}}\right)^{1/3}, \tag{6}$$

$$\varepsilon = -\frac{1}{\rho_w}\frac{d\rho_w}{dz}, \tag{7}$$

where δ_{in} and δ_{out} represent the flow thickness associated with inflow and discharge, respectively (m). Additionally, G is the Froude number for axisymmetric flow (-), θ is the aperture angle of the intake (rad), g is gravity acceleration (m s^{-2}), and ε is the density gradient (m^{-1}). The horizontal speed of water at height z, u (m h^{-1}), is calculated using the values of $q_{in}(z)$ and $q_{out}(z)$ determined by equation 4:

$$u = \frac{q_{in} + q_{out}}{3600s\sqrt{A}}, \tag{8}$$

where s is the thickness of the layer under consideration (m).

2.3 Diffusion coefficient

The diffusion coefficient is computed according to the Munk−Anderson formula (Munk and Anderson, 1948):

$$D_T = D_C = \frac{10}{\sqrt{1+10R_i}}, \tag{9}$$

where R_i is the gradient Richardson number and is defined as

$$R_i = -\frac{g}{\rho_w}\frac{\partial\rho_w}{\partial z}\Big/\left(\frac{\partial u}{\partial z}\right)^2. \tag{10}$$

ρ_w is approximated using the following equation, which is based on Lemmon (2011).

$$\rho_w = 4.3298333\times10^{-5}T^3 - 8.1864490\times10^{-3}T^2 + 6.2139784\times10^{-2}T + 9.9984914\times10^{2}. \tag{11}$$

2.4 Mixing process

The specific water density for each layer is calculated according to equation 11. If the specific water density gradient between layers becomes positive (i.e., $\partial\rho_w/\partial z > 0$), two neighboring layers are mixed. If the specific water density gradient fails to stabilize after the mixing of the two layers, mixing is repeated with the increasing of number of mixing layers until the specific water density gradient becomes stabilized.

2.5 Settling velocity

As for particles, flows are calculated according to the characteristic curve method. The settling velocities of particles are calculated according to Stocks' law, as follows:

$$w = \frac{D_p{}^2\left(\rho_p - \rho_w\right)g}{18\eta}, \tag{12}$$

where D_p is particle diameter (m), ρ_p is particle density (g cm^{-3}), and η is water viscosity (Pa s).

2.6 Ecological model of fecal coliforms (FC) as an indicator of fecal contamination

Both FC and total coliforms (TC) are used as indicators of fecal bacteria, although FC are typically associated with higher cultivation temperatures. Nevertheless, biological reactions involving FC are assumed to be controlled by similar mechanisms to those involving TC. In natural water bodies such as rivers and lakes, it has been shown that the reactivi-

ty of TC (and thus of FC) is limited only by their loss rates (Chapra, 1997), which can be described as follows.

$$\frac{\partial C}{\partial t} = \mu C = -k_b C \quad , \tag{13}$$

where C represents FC concentration (in MPN (100 mL)$^{-1}$) and k_b is the total loss rate (d^{-1}).

In the present study, the total FC loss rate is assumed to be the same as that of TC, which has been described previously (Mancini, 1978; Thomann and Mueller, 1987; Chapra, 1997):

$$k_b = 0.8 \times 1.07^{T-20} + \frac{\alpha \phi_s{}'}{0.55m(z_{sur} - z)}\left(1 - e^{-0.55m(z_{sur}-z)}\right) \quad , \tag{14}$$

where α is a proportionality constant (-), ϕ_s' is surface light energy (ly h^{-1}), m is suspended solids concentration (mg L^{-1}), and Z_{sur} is the height of the water surface (m). The first term on the right-hand side of equation 14 represents the base mortality rate, whereas the second term represents the rate of loss due to solar radiation (i.e., UV disinfection). This latter term is described by the Beer–Lambert law, using the relationship between extinction and suspended solids presented by Di Toro *et al*. (1981).

In the model, FC are divided into two types: a free-floating type (F-FC), and a particle-attached type (P-FC). Loss rates of F-FC due to solar radiation are represented by the second term in equation 13. Similarly, loss rates of P-FC due to solar radiation are typically based loosely on equation 13, although these rates are generally reduced owing to the interception of light before it reaches the particles under consideration. In the present study, the model incorporates a reduction factor (0.5) based on the assumption that particles are ball-shaped and that P-FC are attached uniformly to the surfaces of particles.

2.7 Solar radiation heat

At the water surface, heat loss occurs through evaporation, conduction, and reverse radiation. The net heat loss at the surface, ϕ_L, is defined as

$$\phi_L = \phi_e + \phi_c + \phi_{ra} \quad , \tag{15}$$

where ϕ_e, ϕ_c, and ϕ_{ra} are heat loss by evaporation, conduction, and reverse radiation, respectively. All heat loss values are given in kcal m^{-2} h^{-1}.

The empirical equations adopted for the calculation of heat losses correspond to those of Rohwer and Swinbank (Tsanis *et al*., 2007):

$$\phi_e + \phi_c = \left(1.710965 \times 10^{-5} + 1.027689 \times 10^{-5} W\right) \rho_w \left(e_w - \frac{R_a e_a}{100}\right) \left[L_b + cT + \frac{269.1\left(T - T_a\right)}{e_w - \frac{R_a e_a}{100}} \right] , \tag{16}$$

$$\phi_{ra} = 0.97k\left[\left(T + 273.15\right)^4 - 0.937 \times 10^{-5}\left(T_a + 273.15\right)^6 \left(1.0 + 0.17n\right)\right] , \tag{17}$$

where W is wind speed (m s^{-1}), T_a is air temperature (°C), e_w is saturated vapor pressure at T (hPa), e_a is saturated vapor pressure at T_a (hPa), R_a is relative humidity (%), L_b is the difference in enthalpy between the vapor and liquid states (kcal kg^{-1}), k is the Stefan–Boltzmann constant (4.87654 × 10^{-8} kcal m^{-2} h^{-1}), and n is cloudage (-).

The difference in enthalpy between the vapor and liquid states (Lemmon, 2011) is approximated by the following equation:

$$L_b = 597.7383 - 0.5671T \quad . \tag{18}$$

Heat produced by solar radiation penetrates into the lake water and decays according to the Beer–Lambert law:

$$\phi = \left(1 - \alpha_r\right)\left(1 - \beta\right)\phi_s \exp\left[-\lambda\left(z_s - z\right)\right] , \tag{19}$$

where ϕ_s is solar radiation at the water surface z_s (kcal m^{-2} h^{-1}), α_r is reflectance at the water surface (≈ 0.06), β is ab-

sorbance at the water surface (≈ 0.5), and λ is a decay coefficient (m^{-1}).

2.8 Water–sediment interactions

Particles settling to the bottom of the water body are assumed to become part of the sediment and precipitated suspended solids are not allowed to disturb the water body. No dilution is incorporated into the model.

2.9 Boundary conditions

River inflow volume data are generated from daily observation data. FC and suspended solids (SS) concentrations of inflowing water are described by L–Q equations, as follows:

$$L = aQ^b \ , \tag{20}$$

where L is the load of water quality constituents (g d^{-1} or $\times 10^4$ MPN d^{-1}), Q is the inflow (m^3 s^{-1}), and a and b are constants.

In the model, the percentage of FC represented by F-FC and P-FC depends on SS concentration (Chapra, 1997):

$$FC = FC_F + FC_p \ , \tag{21}$$

$$FC_F = \frac{1}{1+K_d m} FC \ , \tag{22}$$

$$FC_p = \frac{K_d m}{1+K_d m} FC \ , \tag{23}$$

where FC_F and FC_p represent F-FC concentration and P-FC concentrations, respectively (in MPN $(100\ mL)^{-1}$), and K_d is a partition coefficient (m^3 g^{-1}).

Annual fluctuations of river inflow, reservoir effluent, and weather conditions are given as boundary conditions. All input data for calculation step pitch are generated from existing data by linear interpolation. Boundary conditions on the surface of the sediment and the surface of the water body are assumed to be equal to the bottom and top layers, respectively. The discharge volume of the reservoir is calculated from the relationship between observed inflow volume, evaporation from the reservoir surface, precipitation, and fluctuation of reservoir water depth. Air temperature, rain, wind speed, relative humidity, and cloud coverage are referred to the Automated Meteorological Data Acquisition System (AMeDAS) of Japan. Solar radiation is referred to the solar radiation database of the New Energy and Industrial Technology Development Organization (NEDO) of Japan.

2.10 Study reservoir

2.10.1 Overview

The studied reservoir was constructed at the meeting point of two rivers, was filled from late 2002 onward, and has been formally operational since April 2003. The reservoir has a dam body with a height of 63.7 m and has surface area, total storage volume, active storage volume, and catchment area of 910,000 m^2, 11,300,000 m^3, 8,600,000 m^3, and 75.7 km^2, respectively. Water depth at full water level is 59.1 m. Water intake is always taken at 1 m depth near the dam body. Many breeding livestock can be found in the catchment area.

2.10.2 Water sampling and water quality measurements

Monthly observations were conducted at the deepest point of the reservoir, near the dam, and at the two river inflows in 2004. Water samplings were conducted in the morning (10:00–12:00). Sample water was collected at three depths within the reservoir: at the surface (0.5 m depth), from a middle layer (i.e., halfway between the surface and the bottom), and from a bottom layer (1 m above the bottom). Water temperature was measured with a temperature gauge linked long cable. Sample water was collected using a Van Dorn water sampler (VR Type 5042-A, RIGO Co., Ltd), and FC concentration was measured according to the most probable number (MPN) method using EC medium (JWWA, 2011); the minimum probable number was 1.8.

2.11 Simulation conditions

In the model simulations, the L–Q equations ($L = aQ^b$) describing the water quality of the inflow were solved using summing the inflow rate of the two rivers, and water temperature was calculated to be the flow-weighted mean of the two rivers. Coefficients for the L–Q equations are presented in **Table 1**. Water intake depth from the reservoir was set to remain at 0.3 m, and all of the effluents were constrained to flow out from that depth.

Coefficient values are presented in **Table 1**. D_p and ρ_p were assumed heuristically to be 1×10^{-6} m (i.e., 10 μm) and 1.2 g cm^{-3} for F-FC and 3×10^{-5} m (300 μm) and 2.6 g cm^{-3} for SS, respectively. Based on the assumption that P-FC attach primarily to SS, D_p and ρ_p of P-FC were set equal to those of SS.

Input data for each step, q_{in}, q_{out}, T_{in}, C_{in}, and weather conditions were calculated by linear interpolation from the closest before and after data. Calculation was repeated three times continuously using the same annual data set, and a calculation result from the third year was adopted as the simulation result. The outflow from the reservoir (q_{out}) was calculated by a balance of observed values of inflows, reservoir water depths, precipitation, and estimated evaporation. Then, q_{out} was multiplied by 0.5656 from day 306 to day 366 (i.e., from November 1 to December 31) in each calculation year to match the water depths on day 366 (December 31) and on day 1 (January 1) of the next calculation year. Therefore, the verification timescale of the simulation ran from January 1 to October 31.

Ⅲ Results and Discussion

3.1 Observed FC concentrations in the reservoir

Table 2 presents the observed FC concentrations in the reservoir and demonstrates that almost all values were less than 1.8 MPN (100 mL)$^{-1}$, which represents the lower detection limit of the measurement method. FC concentrations in the surface layer were very low. Similarly, FC concentrations in the middle and bottom layers were almost always very low, although higher concentrations (200–300 MPN (100 mL)$^{-1}$) were observed occasionally.

3.2 Annual simulation results for water quality

General remarks regarding the simulation results are first mentioned in this section; then, comparisons between the simulation results and observed values (shown in **Table 1**) are discussed in the next section. **Figure 2** illustrates the simulation results for water depth, water temperature (**Fig.2a**), FC concentration (**Fig.2b**), and SS concentration (**Fig.2c**). The horizontal and vertical axes denote time (in days) after January 1 and the water depth of the reservoir, respectively. The plots show FC and SS concentrations of 0–200 MPN (100 mL)$^{-1}$ (**Fig.2b**) and 0–10 mg L^{-1} (**Fig.2c**), respectively, although only a few points exhibited very high values. **Figure 2** shows that the thermocline formed in late April and persisted until late November (**Fig.2a**), with a seasonal thermocline formed at approximately 10–15 m depth in summer. The deep layers maintained a constant temperature of approximately 4°C throughout the year, except during a period of

Table 1 Coefficient values

			Coefficient value			
			SS	FC	F-FC	P-FC
a	coefficient for L-Q equation	-	1.484	517.73		
b	coefficient for L-Q equation	-	2.370	0.622		
k_d	partition coefficient	(m^3 g^{-1})				0.06
α	proportionality constant	(-)			0.4	0.4
n	reduction factor	(-)				0.5
D_p	particle diameter	($\times 10^{-6}$m)	30		1	30*
ρ	particle density	(g cm^{-3})	2.6		1.2	2.6*

*P-FC = SS, assuming P-FC attach primarily to SS surface

Table 2 Observed FC concentrations in the reservoir (2004)

	fecal coliforms (FC, MPN (100 mL)$^{-1}$)		
	surface	middle	bottom
Apr. 23	<1.8	<1.8	<1.8
May 11	<1.8	11	<1.8
Jun. 9	<1.8	<1.8	<1.8
Jul. 21	<1.8	220	<1.8
Aug. 4	<1.8	2	<1.8
Aug. 18	<1.8	<1.8	9
Sep. 10	<1.8	<1.8	<1.8
Sep. 29	<1.8	<1.8	2
Oct. 20	2	<1.8	270

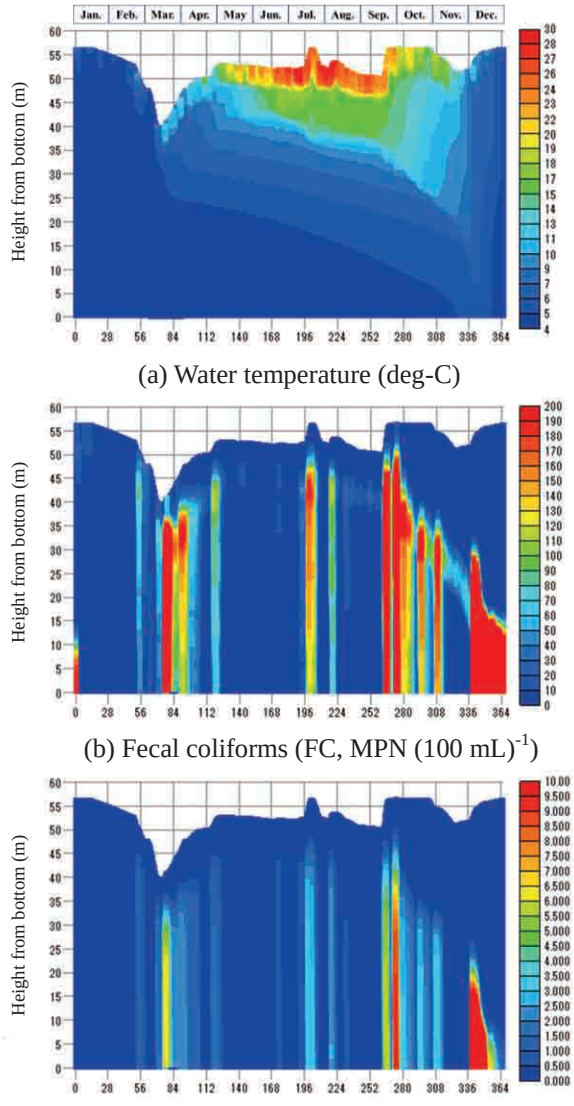

(a) Water temperature (deg-C)

(b) Fecal coliforms (FC, MPN (100 mL)$^{-1}$)

(c) Suspended solids (SS, mg L^{-1})

Fig.2 Simulated annual water quality fluctuation

mixing that lasted from late November to early December. This phenomenon is common in reservoirs of this type.

FCs were introduced into the reservoir only through the influent, with no additional growth within the reservoir in the simulation. Accordingly, FC concentrations were generally low and increased in response to increased influent flow (**Fig.2b**). In the layers near the surface, FC concentrations were almost zero for the majority of the time, likely owing to

FC loss due to solar radiation (UV disinfection). These results agree with the observed values (**Table 1**). The FC fraction attached to particles (P-FC) settled along with SS immediately (i.e., within a few days) after being introduced into the reservoir (**Fig.2c**). Thus, the transport of P-FC to depth within the reservoir was more pronounced than that of F-FC. Moreover, the UV disinfection rate of P-FC is half that of F-FC owing to particle shading. Accordingly, despite the dominance of P-FC in the reservoir as a whole, the settling of P-FC occurred in contrast to the concentration of F-FC in the upper parts of the reservoir. In particular, the majority of F-FC became concentrated between the first and seasonal thermoclines, in a layer approximately 5–20 m below the surface, during the summer irrigation season. Overall, FC concentrations tended to be higher below the depth of the daily thermocline, particularly after large inflows.

3.3 Comparison between observed and simulated vertical water quality profiles

Simulation results were verified based on their conformance with observed values on July 21 (day 203 in the simulation) and October 20 (day 296), when the maximum FC concentrations were observed (**Table 1**). **Figure 3** presents comparisons between the observed (circles) and simulated (lines, 12:00) values for temperature on July 21 (**Fig.3a**), FC concentration on July 21 (**Fig.3b**), temperature on October 20 (**Fig.3c**), and FC concentration on October 20 (**Fig.3d**). Water quality indicators and the water depth of the reservoir are shown on the horizontal and vertical axes, respectively. Water depth was 55.8 m and 56.2 m on July 21 and October 20, respectively. FC values below the limit of detection (<1.8 MPN (100 mL)$^{-1}$) are plotted as 1.8 MPN (100 mL)$^{-1}$.

For the other observation day of shown in **Table 2** the simulation results for FC concentrations in the bottom, middle, and surface layers are all lower than 0.21 MPN (100 mL)$^{-1}$, except for September 29, and there are similar to observed values. The simulation result for September 29 appears to have been overestimated: it was approximately 500 MPN (100mL)$^{-1}$ around the middle layer. This discrepancy can be attributed to the overestimation of FCs and SS for inflows (calculated according to the L–Q equations) when the reservoir received very large inflows (see the surface elevation in late September; **Fig.2**).

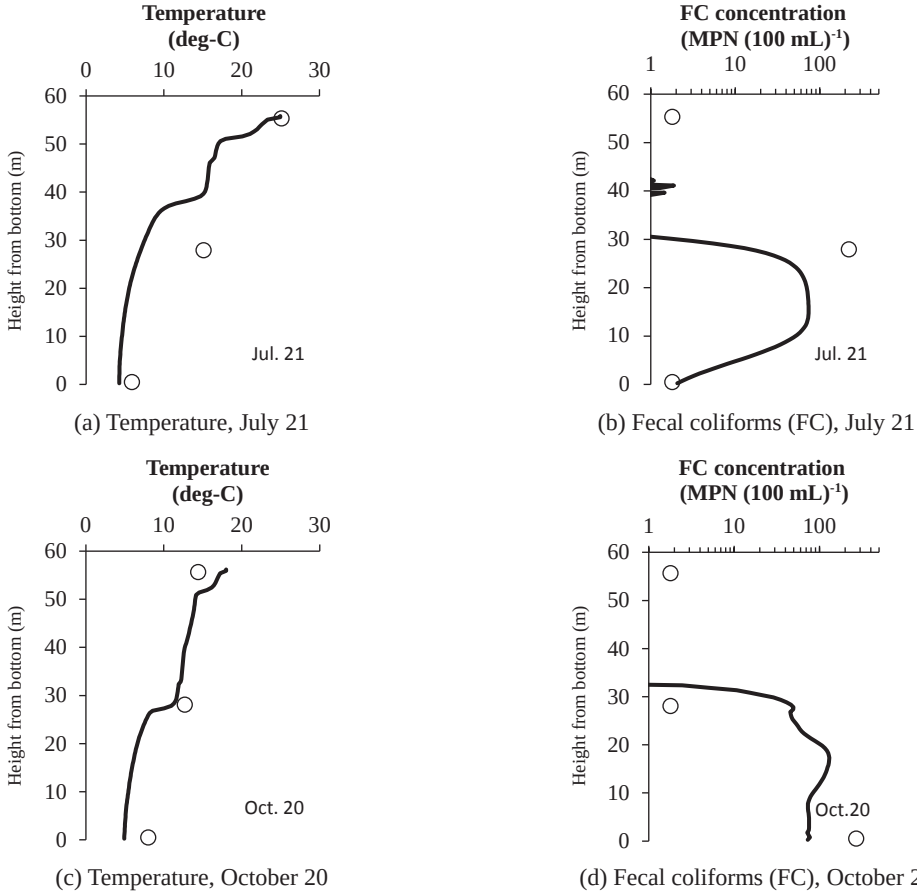

(a) Temperature, July 21

(b) Fecal coliforms (FC), July 21

(c) Temperature, October 20

(d) Fecal coliforms (FC), October 2

Fig.3 Comparison of simulated and observed vertical profiles of water quality in the reservoir for different days

The simulated water temperatures illustrate clearly the daily and seasonal thermoclines on July 21 (**Fig.3a**) and October 20 (**Fig.3c**). Although the seasonal thermocline simulated on July 21 was shallower than that observed (**Fig.3a**), the simulated water temperature was considered to reproduce the observed data successfully.

The simulated FC concentrations indicate interesting results for both of the days studied. On July 21, higher FC concentrations were observed in the middle layer, corresponding approximately to the peak in FC concentration in the lower middle layer in the simulation results (**Fig.3b**). Moreover, FC concentrations were similar in the bottom layer for both the simulated and observed results. The small peak in simulated FC concentrations around 40 m from the bottom can be attributed to the accumulation of F-FC, as described above. While very large inflows were observed in late July, as in late September, the simulation result for July 21 can be considered appropriate and is not associated with any overestimation of FC concentrations. This may indicate that a seasonal coefficient is required in the L–Q equation describing FC concentration. On October 20, the simulated FC concentrations in the bottom layer underestimated the observed values, whereas FC concentrations in the middle layer were below the detection limit for both the simulated and observed distributions (**Fig.3d**). FC concentrations in reservoirs can vary by up to several orders of magnitude; for example, observed FC concentrations in this study cover a wide range (<1.8 to 270 MPN (100 mL)$^{-1}$). In contrast, quantitative mismatches between the simulation results and observed values (**Fig.3b** and **Fig.3d**) are typically within one order of magnitude; this degree of accuracy is considered to be reasonable for simulation of FC concentration. In this context, the comparisons shown in **Fig.3** demonstrate the validity of the model developed here. Nonetheless, the results seem to suggest that the model requires further tuning, particularly in its treatment of parameters such as SS size distribution and the consideration of seasonality in the L–Q equations use to describe FC load. Such tuning should be conducted in future to refine the model further.

Ⅳ Conclusions

In the present study, a numerical model has been developed to simulate the vertical profiles of fecal coliforms in reservoirs. Based on a comparison of the simulation results obtained using this model with observed data describing FC concentrations, it is concluded that the model exhibits reasonable reproducibility for almost every comparison and is applicable for use in a reservoir setting. Accordingly, this model will be useful in the management of reservoir water intake and in monitoring contamination by fecal bacteria, which can be introduced into reservoirs through agricultural runoff and domestic effluent. In Japan, the diversification of water use is widespread and fecal contamination may be increased by such diversification, particularly in the case of recycled water. Thus, the monitoring and management of fecal contamination, which can be achieved by models such as the one described here, are likely to be critical to maintaining a safe and reliable supply of water.

Acknowledgements

We would like to extend our thanks to everyone who assisted in the collection of field data.

Reference

1) Aki, S., O. Shimoda, T. Shirasuna, T. Akasaki, Y. Miyanaga and M. Sakata (1981) Reservoir Water Quality -- Investigation and Analysis, CRIEPI Research Report No.302, Central Research Institute of Electric Power Industry. (in Japanese with English abstract)
2) Canale R. P., M. T. Auer, E. M. Owens, T. M. Heidtke and S. W. Effler (1993) Modeling fecal coliform bacteria - II. Model development and application, *Water Research*, **27**, 703-714.
3) Chapra S. C. (1997) Surface Water-Quality Modeling, Waveland Pr Inc.
4) Di Toro, D. M., D. J. O' Connor, R. V.Thomann and J. P. St. John (1981) Analysis of fate of chemicals in receiving waters. Phase 1. Chemical Manufacturers Association, HydroQual Inc.
5) Hamada K., T. Hitomi, T. Kubota and E. Shiratani, (2010) Fluctuation and Transportation of Indicator Microorganisms in the Agricultural Irrigation System, *Proc. of Annual Meeting of The Japanese Society of Irrigation, Drainage and Rural Engineering*, 744-745. (in Japanese)

6) JWWA (2011) Water Examination Methods of Japan (2011 Edition), Japan Water Works Association.
7) Lemmon, E.W. (2011) Thermophysical properties of water and steam, CRC Handbook of Chemistry and Physics, 91st edition, CRC Press, pp. 6-1 - 6-4.
8) Mancini, J. L. (1978) Numerical estimates of coliform mortality rates under various conditions, *Journal of Water Pollution Control Federation*, **50**(11). 2477-2484.
9) Momii, K. and Y. Ito (2008) Heat budget estimates for Lake Ikeda, *Japan. Journal of Hydrology* 361: 362-370.
10) Munk, W. and E. Anderson (1948) Notes on the theory of the thermocline. *Journal of Marine Research*, 7: 276-295.
11) Steets B. M. and P. A. Holden (2003) A mechanistic model of runoff-associated feacal coliform fate and transport through a coastal lagoon, *Water Research*, **37**, 589-608.
12) Suh C.W., J. W. Lee, Timothy Hong Y. S. and H. S. Shin (2009) Sequential modeling of fecal coliform removals in a full-scale activated-sludge wastewater treatment plant using a evolutionary process model induction system, *Water Research*, **43**, 137-147.
13) Thomann and Mueller, 1987
14) Tsanis, IK, J. Wu, H. Shen and C. Valeo (2007) Environmental Hydraulics - Hydrodynamic and Pollutant Transport Modelling of Lakes and Coastal Waters, Elsevier.
15) WHO (2006) WHO Guidelines for the Safe Use of Wastewater, Excreta and Greywater - Volume II, Wastewater Use in Agriculture.

Received: 9 December 2013

ダム湖における糞便性大腸菌群の鉛直分布に関する数値解析法の開発

濵田康治*，白谷栄作**，久保田富次郎*，人見忠良*
*水利工学研究領域 水環境担当
**企画管理部 研究調整役

要　約

鉛直一次元のレイヤーモデルによりダム湖内での糞便性大腸菌群の動態を解析した。糞便性大腸菌群を浮遊態と土粒子に付着したものの2種類に分別した。土粒子の沈降を特性曲線法により解析することで、糞便性大腸菌群が土粒子とともに移動・沈降する糞便性大腸菌群の動態を考慮可能とした。集水域に畜産牧場があり降雨時に糞便性大腸菌群の流入が増大するダム湖を対象とした実測値とモデルシミュレーション結果との比較により、提案したモデルがダム湖最深部地点での糞便性大腸菌群数実測値の鉛直プロファイルを良好に再現可能であること示した。また、モデル解析の結果から、糞便性大腸菌群は出水イベント直後を除き湖水中での著しい濃度上昇が見られないこと、浮遊態の糞便性大腸菌群が日躍層と季節躍層の間に低濃度であるが浮遊する傾向があること、土粒子付着態の糞便性大腸菌が流入後速やかに沈降し、出水イベント直後に深部において高濃度で存在する傾向があることが示された。

キーワード：鉛直一次元レイヤーモデル、糞便性大腸菌群、鉛直プロファイル